Heliyon 9 (2023) e16702

Contents lists available at ScienceDirect

Heliyon

journal homepage: www.cell.com/heliyon

Optimal selection of b-values for differential diagnosis of mediastinal lymph nodes using diffusion-weighted imaging

Li-Ping Qi [a,b], Zheng Zhong [b,e], Ying-Shi Sun [a], Xiao-Ting Li [a], Lei Tang [a], Xiaohong Joe Zhou [b,c,d,e,*]

[a] Department of Radiology, Key Laboratory of Carcinogenesis and Translational Research, Ministry of Education, Peking University Cancer Hospital and Institute, Beijing, China
[b] Center for Magnetic Resonance Research, University of Illinois at Chicago, Chicago, IL, USA
[c] Department of Radiology, University of Illinois at Chicago, Chicago, IL, USA
[d] Department of Neurosurgery, University of Illinois at Chicago, Chicago, IL, USA
[e] Department of Biomedcial Engineering, University of Illinois at Chicago, Chicago, IL, USA

ARTICLE INFO

Keywords:
Thorax
Lymph nodes
Differential diagnosis
Diffusion magnetic resonance imaging

ABSTRACT

This study proposed to investigate the optimal selection of b-values in diffusion-weighted imaging for distinguishing malignant from benign mediastinal lymph nodes. Diffusion-weighted imaging with six b-values was performed on 35 patients at 1.5 T. Image quality score, signal-to-noise ratio, and relative contrast ratio of lymph node to chest muscle were compared between the diffusion-weighted images with a b-value up to 800 and 1000 s/mm^2. Using a lower and an upper b-value in the range of 0–1000 s/mm^2, eight apparent diffusion coefficient maps were obtained from a mono-exponential model. Receiver operating characteristic analysis was employed to evaluate the performance of the apparent diffusion coefficients for distinguishing malignant from benign mediastinal lymph nodes by using the area under the curve as a criterion.

The mean image quality score and the relative contrast ratio showed no difference between b-values of 800 and 1000 s/mm^2. In the receiver operating characteristic analysis, the areas under the curve of apparent diffusion coefficient with b-value pairs of (0, 800), (0, 1000), and (50, 800) s/mm^2 were significantly higher than those from the other b-value pairs. No significant difference was observed among the three b-value pairs. Apparent diffusion coefficient obtained from b-value pairs of (0, 800), (0, 1000), and (50, 800) s/mm^2 showed superior diagnostic performance compared to the other b-value combinations. Based on several practical considerations, the b-value pair of (50, 800) s/mm^2 is recommended for differential diagnosis of mediastinal lymph nodes.

1. Introduction

With its sensitivity to water diffusion in tissues, diffusion-weighted imaging (DWI) has been widely used to probe changes in microstructures, cellularity, and microenvironment during disease progression and regression. This imaging technique is valuable for detecting or characterizing a number of tumors [1]. In particular, the importance of DWI for discriminating malignant versus benign

* Corresponding author. ; Center for MR Research, University of Illinois at Chicago; 2242 West Harrison Street, Suite 103, M/C 831, Chicago, IL 60612, USA.
E-mail address: xjzhou@uic.edu (X.J. Zhou).

https://doi.org/10.1016/j.heliyon.2023.e16702
Received 6 September 2022; Received in revised form 16 April 2023; Accepted 24 May 2023
Available online 26 May 2023

lymph nodes has been demonstrated in several studies [2–6].

Despite encouraging results, the published studies exhibit a considerable variability in the selection of b-value – a critical parameter in DWI for both qualitative and quantitative image interpretation. The inconsistent use of b-values leads to different cut-off thresholds of apparent diffusion coefficient (ADC) for discriminating malignant versus benign mediastinal lymph nodes (MLN), causing variable and confusing diagnostic performance. To the best of our knowledge, no study has reported the optimal selection of b-values for differential diagnosis of MLN using DWI.

Theoretically, DWI with the highest possible b-value can minimize the effect of T2-shine through (e.g., from blood supply) and increase the sensitivity to slow diffusion. Due to the need for preserving signal-to-noise ratio (SNR) and the limitation imposed by the gradient strength, b-value in the range of 800 s/mm^2 to 1000 s/mm^2 is commonly used as an upper bound for evaluating MLN [3,4]. When computing ADC, this upper-bound b-value is often employed jointly with a lower b-value, which is needed to suppress the perfusion contribution to the signal in vasculature-rich tissues [7]. At present, the choice of the high and low b-value pair is somewhat arbitrary. The aim of this study is to investigate the optimal selection of the b-value pair for distinguishing malignant from benign MLN.

2. Materials and methods

2.1. Patients

The institutional review board of Peking University Cancer Hospital and Institute approved this prospective study and written informed consent was obtained from all patients. The inclusion criteria were: 1. Presence of enlarged lymph nodes in the mediastinum detected by CT (short axis $\geq$8 mm); 2. Patients with clinically motivated biopsy or resection of MLN for disease diagnosis or treatment; 3. No invasive examinations or antitumor treatment performed prior to MRI; and 4. No contraindications to MRI scans (e.g., cardiac pacemaker, MRI-incompatible surgical clips, metallic implants, or prosthetic devices). The exclusion criteria consisted of: 1. Lack of pathologic or other diagnosis of MLN; 2. Hypointensity of the enlarged MLN on T2-weighted images, which is a typical benign feature; 3. poor quality of DWI images (e.g., excessive motion artifacts, low SNR, etc.); or 4. Insufficient solid area in the MLN for placing a region of interest (ROI). Between July of 2014 and June of 2015, a total of 35 subjects met all inclusion criteria and none of the exclusion criteria. The detailed characteristics of the patients are summarized in Table 1.

2.2. Diagnostic criteria

The pathologic diagnoses of MLN were made by mediastinoscopy or mediastinal lymphadenectomy in 23 cases, transbronchial needle aspiration biopsy in 6 cases, CT-guided core-needle biopsy in 4 cases, supraclavicular lymph node resection in 1case. One remaining case of sarcoidosis was proven with follow-up radiologic examination after one month of steroid therapy that revealed significant regression of the nodules. There were 23 non-small cell lung cancers (NSCLC), including 17 adenocarcinomas, 4 squamous cell carcinomas, 1 adeno-squamous carcinoma, and 1 NSCLC without specialized pathological type. A total of 91 nodes from the 35 patients were analyzed, including 49 malignant and 42 benign nodes.

2.3. Image acquisition

All patients were scanned on a 1.5 T Siemens Aera MR scanner (Siemens Healthineers, Erlangen, Germany) with an eight-channel phased-array body coil. The MRI examinations were performed with the patients in the supine position by using a stack of 28–36 transverse slices to cover the mediastinal area of the thorax. Prior to DWI, transverse T2-weighted turbo spin echo (TSE) images with ECG-gating were acquired. The key imaging parameters were: TR = 6 *R*–R intervals, TE = 86 m s, slice thickness = 5 mm, slice gap = 1 mm, field of view = 32–38 cm, phase FOV = 100%, pixel size $\approx$1 $\times$ 1 mm^2, turbo factor = 25, and scan time = 3 min 15 s.

DWI with six b-values (0_1, 50_1, 100_1, 200_1, 800_4, and 1000_4 s/mm^2 with the subscript denoting the number of averages) was performed by using a single-shot spin-echo echo-planar imaging sequence in the transverse plane. The slice locations of DWI were copied from the T2-weighted images to facilitate anatomic correspondence. For each non-zero b-value, the diffusion gradient was applied successively along each of the three orthogonal directions, producing a trace-weighted image to minimize the influence of diffusion anisotropy. The other acquisition parameters were: TR = 9600 ms, TE = 62 ms, FOV $\approx$320–380 mm, FOV phase = 80%, bandwidth = 2180 Hz/pixel, pixel size $\approx$2.3 $\times$ 2.3 mm^2, slice thickness = 5 mm, slice gap = 1 mm, and scan time = 5 min 55 s for the six b-values.

Table 1
Patient characteristics and clinical diagnoses.

Male: Female	16:19	35 (total)
Age (years)	59.4 $\pm$ 9.3 (average)	38–76 (range)
Malignant diseases	NSCLC	23
	Small-cell lung cancer	1
	Lymphoma	2
Benign diseases	Tuberculosis	2
	Inflammation or Granulomatous inflammation	4
	Sarcoidosis	3

2.4. Qualitative evaluation

Diffusion-weighted (DW) images with b-values of 800 s/mm^2 and 1000 s/mm^2 from the 35 patients were evaluated independently by two chest radiologists with reference to T2-weighted images. The images were presented randomly to the readers who were blinded of the b-value information. The main factors considered for image quality included SNR, artifacts, and distortion. A 4-point scoring scale was used in the qualitative assessment: score = 1 when poor image quality precluded assessment of the target lesions; score = 2 when image quality was not good but still useable; score = 3 when image had only minor degradation that did not affect lesion evaluation; score = 4 when image quality was excellent without any problem noted.

2.5. Quantitative evaluation

The diffusion images were analyzed without the knowledge of pathologic results of the lymph nodes under study. An ROI was manually placed on the maximum cross-sectional area on the ADC map computed from all b-values (Fig. 1), as recommended by Joo et al. [8]. Necrotic regions were excluded from the ROI by verifying against the corresponding T2-weighted image. The mean value of ADC among the voxels within the ROI was recorded for each node. Up to three lymph nodes were analyzed from each patient. The locations of MLN on the T2-weighted images and the corresponding DW images were paired and labeled in consultation with the operating surgeon immediately after the operation, which ensured that the lymph nodes evaluated by pathology matched precisely with those studied by imaging.

The signal intensity (SI) of DW images with b of 800 s/mm^2 and 1000 s/mm^2 was extracted from each lymph node. To measure the background noise, two oval or circular ROIs (>100 mm^2) were placed away from the imaged subject in the same slice where the ROI for the MLN was drawn. The averaged standard deviation (SD) from the two ROIs was used to calculate the SNR according to the following equation:

$$SNR = SI_{lymph\_node}/SD_{background}. \quad [1]$$

To calculate a relative contrast ratio (rCR) of lymph node to chest muscle, an oval or circular ROI in the rhomboid muscle (>20 mm^2) was drawn in the same slice as the MLN under study. The rCR of lymph node to chest muscle was then computed as:

$$rCR = (SI_{lymph\_node} - SI_{muscle})/\ SI_{muscle}, \quad [2]$$

where SI is the signal intensity of the tissue indicated by the subscript.

2.6. ADC analyses

Using one b-value in the lower range (i.e., 0–200 s/mm^2) and another in the upper range (i.e., 800 or 1000 s/mm^2), a total of eight ADC maps were obtained from a mono-exponential diffusion model:

$$S_{high} = S_{low} \times e^{-\Delta b(ADC)}, \quad [3]$$

where S_{high} and S_{low} are the signal intensities corresponding to the high and low b-value images, respectively, and $\Delta b = b_{high} - b_{low}$.

2.7. Statistical analyses

Statistical analyses were conducted using SPSS software version 24.0 (SPSS/IBM, Chicago, IL, USA) and MedCalc version 12.3.0.0 (MedCalc Software, Mariakerke, Belgium). A Mann-Whitney *U* test was used to detect the difference in image-quality score between DWI with b-values of 800 s/mm^2 and 1000 s/mm^2, followed by a paired-t test to detect differences in rCR between the DW images acquired with the two b-values. To compare the difference in SNR and rCR between the benign and the malignant groups with either b-value, a Mann-Whitney *U* test was employed for non-normal distributions. For normal distributions, an independent sample *t*-test was

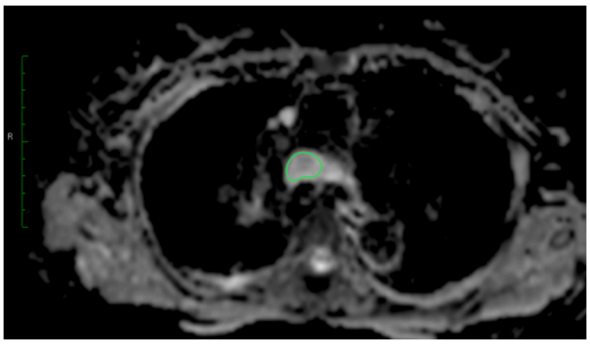

Fig. 1. An illustration of an ROI drawn over a mediastinal lymph node on the ADC map.

used instead to detect differences in ADCs computed from all b-value pairs between malignant and benign lymph nodes. A receiver operating characteristic (ROC) analysis was employed to evaluate the performance of each of the ADC maps obtained from different b-value pairs. The area under the ROC curves (AUC) was compared using a DeLong method, and the optimal cutoff value was determined at the maximum Youden index. A weighted kappa coefficient was calculated to evaluate inter-observer agreement. 0.00–0.20, 0.21–0.40, 0.41–0.60, 0.61–0.80, 0.81–1.00 were considered as poor, fair, moderate, substantial and perfect agreement, respectively. In all analyses, statistical significance was declared when $p < 0.05$.

3. Results

Fig. 2 shows a set of representative DW images acquired with four b-values in the lower range (0–200 s/mm^2) and two in the upper range (800–1000 s/mm^2). The images were obtained from a patient with a histologically confirmed benign MLN at station 4R. One b-value in the lower range and another in the upper range were used to calculate ADC according to Equation [3], resulting in a total of eight ADC maps as shown in Fig. 3 for this representative patient.

3.1. Qualitative evaluation

All DW image quality scores were 2 or above. The mean score with b-value of 800 s/mm^2 showed no significant difference from that with b-value of 1000 s/mm^2 (3.51 ± 0.65 vs 3.43 ± 0.70, $p = 0.291$). A moderate inter-observer agreement was observed with Kappa value of 0.547, 0.511 for DW image with b-value of 800 s/mm^2 and 1000 s/mm^2, respectively.

3.2. Quantitative evaluation

As expected, the mean SNRs with b-value of 800 s/mm^2 were higher than that with b-value of 1000 s/mm^2 for both benign and malignant MLN (37.35 vs 34.01; 129.50 vs 108.80, respectively). In addition, the coefficient of variation (CV) of SNR on DW images with $b = 800$ s/mm^2 was smaller than that with $b = 1000$ s/mm^2 for both the benign and malignant groups (0.48 vs 0.54; 0.62 vs 0.80).

The rCR (i.e., lymph node to chest muscle) showed no difference between DW images with $b = 800$ s/mm^2 and 1000 s/mm^2 ($p = 0.058$). However, the rCR between the malignant and benign groups differed significantly with either $b = 800$ s/mm^2 (3.17 ± 1.17 vs 0.70 ± 0.63; $p < 0.001$) or $b = 1000$ s/mm^2 (3.37 ± 2.04 vs 0.76 ± 0.56; $p < 0.001$), as shown in Fig. 4.

3.3. ADC and ROC analysis

The mean ADC value of the malignant MLN was significantly lower than that of the benign group for all b-value pairs except for (200, 1000 s/mm^2) ($p = 0.06$ for 200–1000 s/mm^2; $p \leq 0.001$ for all other b-value pairs).

The results from the ROC analysis are summarized in Table 2 and Fig. 5. The ADC computed with b-values of (0, 800 s/mm^2) produced the largest AUC (0.941), which matched the AUC when all b-values were used to obtain ADC. In addition, the b-value pairs of (0, 1000 s/mm^2) and (50, 800 s/mm^2) produced a higher AUC ($\geq$0.888) than the remaining b-value pairs for differentiating malignant from benign MLN.

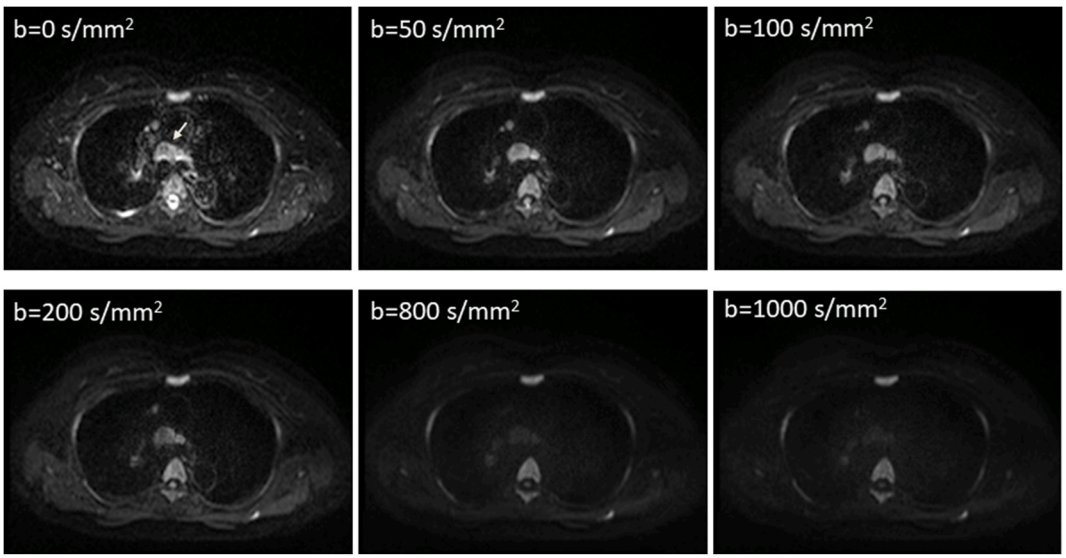

Fig. 2. A set of representative DW images acquired with four b-values in the lower range (0–200 s/mm^2) and two in the upper range (800–1000 s/mm^2), as annotated. The patient had a histologically confirmed benign MLN at station 4R (white arrow).

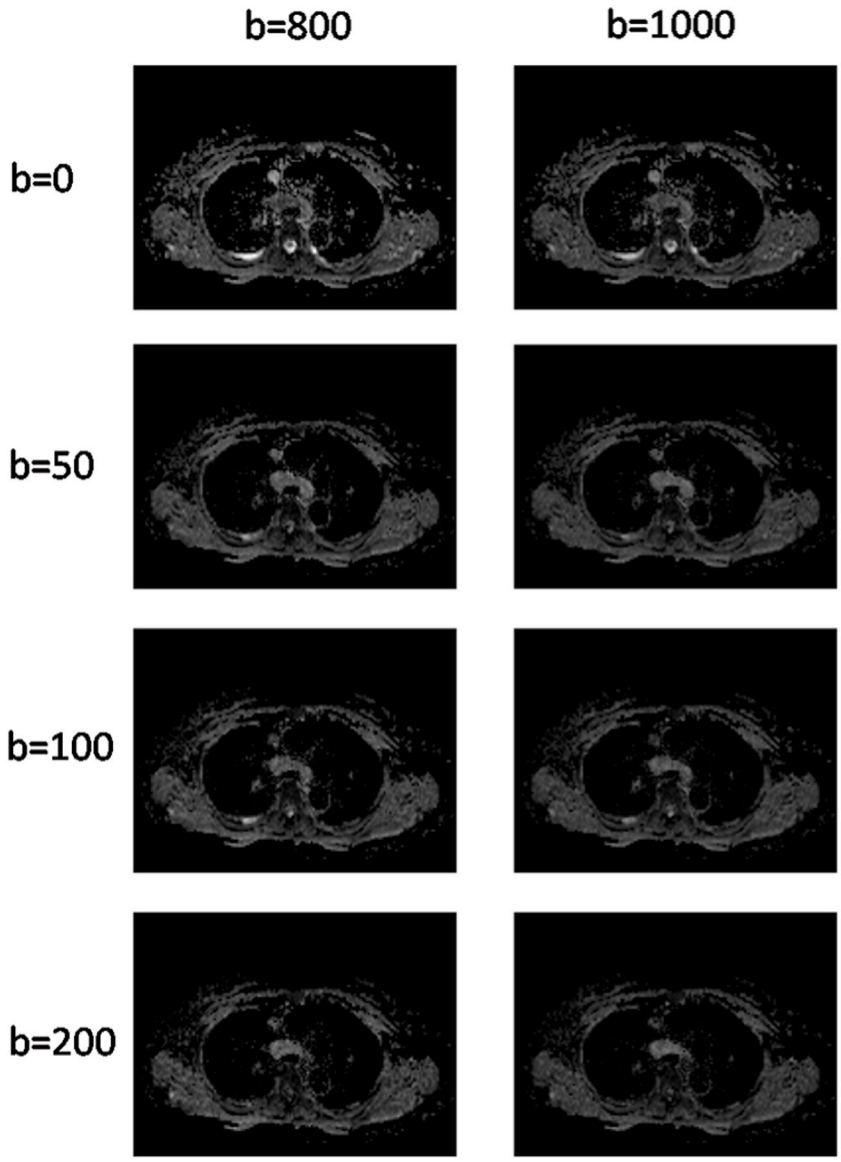

Fig. 3. A set of eight ADC maps computed with different b-value pairs using one b-value in the lower range (0–200 s/mm^2) and another in the upper range (800 or 1000 s/mm^2) for the representative patient in Fig. 1. The units of b-values in the figure are s/mm^2.

The AUC results obtained from different b-value pairs (with $p < 0.05$ for MLN differentiation) are further compared in Table 3 where the p-values for different comparisons are shown. The AUCs of ADC with b-value pairs of (0, 800 s/mm^2), (0, 1000 s/mm^2), (50, 800 s/mm^2), as well as with all b-values, were higher than the others, but exhibited no significant difference among these b-value combinations. The AUC of ADC with b of (200, 800 s/mm^2) was significantly lower than the other AUCs. The AUCs of ADC with b of (100, 800 s/mm^2) and (100, 1000 s/mm^2) were statistically different from those with b-value pairs of (0, 800 s/mm^2), (0, 1000 s/mm^2), as well as with all b-values, except for the AUCs between b-value pairs of (100, 800 s/mm^2) and (0, 1000 s/mm^2).

For the three b-value pairs that gave larger AUCs (i.e., AUC $\geq$0.888), the cut-off values of ADC, sensitivity, specificity, and diagnostic accuracy are listed in Table 4. For comparison, the descriptive statistics when all b-values were used is also included in the table. With a cutoff value of 1.66×10^{-3} mm^2/s, the ADC with the b-value pair of (0, 800 s/mm^2) provided the highest diagnostic sensitivity (90.5%), specificity (89.8%) and diagnostic accuracy (89.0%), surpassing the performance even when all b-values were used. This finding can be further seen in the ROC curves in Fig. 4.

4. Discussion

Although DWI based on two b-values has been suggested for differentiating malignant versus benign MLN, there has not been a

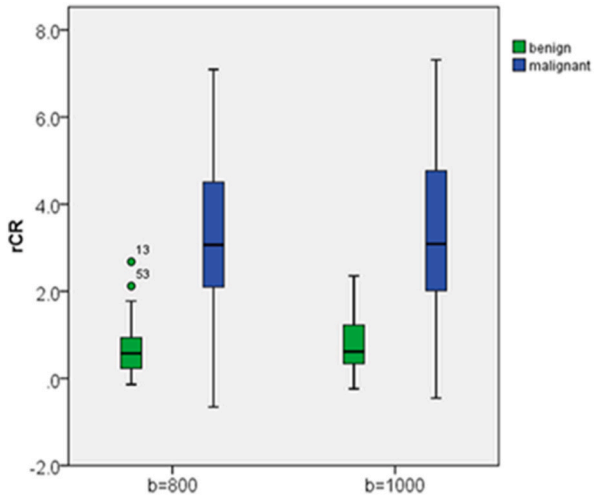

Fig. 4. Relative contrast ratio (rCR) between lymph nodes and chest muscle for the benign (green) and malignant (blue) groups, as measured from the DW images with b-value of 800 s/mm^2 (left) and 1000 s/mm^2 (right).

Table 2
AUC from an ROC analysis on the ADC values obtained from different b-value pairs for differentiating malignant from benign MLNs.

b-value pair (s/mm^2)	AUC	p-value	95% CI
0, 800	0.941	<0.001	0.896–0.987
0, 1000	0.924	<0.001	0.873–0.974
50, 800	0.888	<0.001	0.820–0.957
50, 1000	0.809	<0.001	0.721–0.897
100, 800	0.844	<0.001	0.760–0.927
100,1000	0.760	<0.001	0.660–0.861
200, 800	0.675	0.004	0.562–0.788
200,1000	0.615	0.060	0.496–0.733
multi-b	0.941	<0.001	0.897–0.985

"Multi-b" indicating ADC obtained from all b-values.

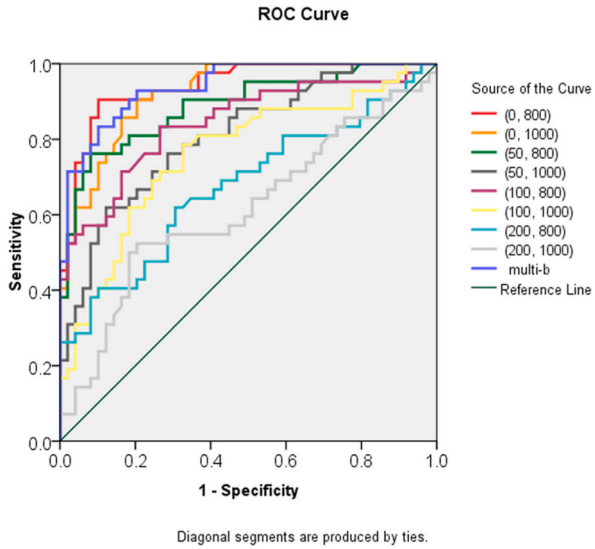

Fig. 5. ROC curves of using ADC obtained from different b-value pairs for differentiating malignant from benign MLNs. For comparison, the ROC curve of using ADC obtained from all b-values is also shown and labeled as "multi-b". In the figure legend, the units for the b-values are s/mm^2.

Table 3
Summary of the p-values when comparing AUC of ADC obtained from different b-values.

ADC with	multi-b	0,800	0,1000	50,800	50,1000	100,800	100,1000	200, 800
multi-b	NA	0.9751	0.3901	0.9751	0.001	0.0109	<0.001	<0.001
0, 800	–	NA	0.3515	0.1213	0.058	0.0219	0.0013	<0.001
0, 1000	–	–	NA	0.3503	0.041	0.0645	0.001	<0.001
50, 800	–	–	–	NA	0.007	0.2674	0.0195	0.0001
50, 1000	–	–	–	–	NA	0.6133	0.2958	0.0136
100, 800	–	–	–	–	–	NA	0.0155	0.018
100,1000	–	–	–	–	–	–	NA	0.1594

"Multi-b" indicating ADC obtained from all b-values.

Table 4
Diagnostic performance of using ADC to differentiate malignant from benign MLNs.

ADC with	cut off ($\times 10^{-3}$ mm^2/s)	sensitivity	specificity	accuracy
0, 800	1.66	90.5	89.8	89.0
0, 1000	1.52	90.5	79.6	84.6
50, 800	1.55	76.2	89.8	84.6
multi-b	1.43	81.6	88.1	85.7

"Multi-b" indicating ADC obtained from all b-values.

comprehensive study on how to select the b-values to achieve an optimal result. This study demonstrates that three b-value pairs, (0, 800 s/mm^2), (0,1000 s/mm^2), and (50, 800 s/mm^2) outperformed the other b-value combinations in the range of b = 0–1000 s/mm^2. In addition, we have observed no difference in image-quality scores or rCR between the DW images acquired with b-value of 800 and 1000 s/mm^2, and significance differences in rCR and ADC between malignant and benign MLN with either b-value. These results, although empirical in nature, fill in a knowledge gap and can help improve the reliability of using DWI for discriminating malignant versus benign MLN.

When choosing proper b-values, the SNR and contrast should be considered [9,10]. A higher b-value typically results in a reduced SNR not only because of increased signal attenuation due to diffusion but also increased TE (hence additional signal loss due to T2 decay) when the maximal gradient strength is used, as is often the case for DWI. For these reasons, the upper limit for this study was set at 1000 s/mm^2, which is consistent with the majority of clinical DWI protocols [11,12]. Contrast in lesion detection with respect to the background tissues is another important consideration when choosing an optimal b value in DWI [7,13–16]. We investigated the rCR between lymph nodes and chest muscle, and observed no difference in rCR between DW images with b-values of 800 s/mm^{2}and 1000 s/mm^2, likely because of the potential gain in rCR at the higher b-value was masked by the reduced SNR.

ADC measurement has been increasingly applied to differential diagnosis of malignant versus benign diseases [1,3,4,17]. Our results showed that the mean ADC of malignant MLN was significantly lower than that of the benign lesions for all b-value pairs investigated except for (200, 1000 s/mm^2). These results are largely consistent with what was reported in previous studies [2,5,6,18, 19]. Malignant lymph nodes have denser cellularity, higher nucleus-to-cytoplasm ratios, and more limited extracellular space compared to inflammatory lymph nodes and benign hyperplasia, as pathologically proven in a metastatic breast cancer model [20]. It is worth noting that a low ADC can be also observed in lesions (e.g., fibrosis) other than tumor. Therefore, in this study we excluded MLN exhibiting low signal (caused by fibrosis or calcification) on T2-weighted images. With this exclusion, an AUC as high as 0.941 was achieved with the b-value pair of (0, 800 s/mm^2), indicating an excellent diagnostic accuracy.

Similar performance in AUC was also observed in two other b-value pairs: (50, 800 s/mm^2) and (0, 1000 s/mm^2). These results suggest that all the three b-value pairs could be used for DWI to discriminate MLN. Inclusion of b = 0 s/mm^2 as the lower bound can make the DWI protocol susceptible to perfusion effects as dictated by the IVIM model [21] and an upper bound of b = 1000 s/mm^2 can suffer from additional SNR loss. Because of these reasons, the b-value pair of (50,800 s/mm^2) is recommended within the range of b-values we have investigated.

In a previous study [22], a b-value set of 250–1000 s/mm^2 was suggested to obtain ADC free from perfusion for characterizing non-small cell lung cancer. In another study, it was recommended that at least two b-values should be used to measure ADC with one b-value greater than100 s/mm^2 and the other between 500 and 1000 s/mm^2. Contrary to these recommendations, our result showed that ADCs computed from b-value pairs of (200, 1000), (200, 800), (100, 800) and (100, 1000) s/mm^2 showed poorer diagnostic performance for differential diagnosis of MLN. One possible explanation is that MLNs are embedded in mediastinal fat which has relatively low blood supply. Thus, the influence from perfusion effect is less profound comparing to other organs, allowing a lower b-value (0 or 50 s/mm^2) be used for differential diagnosis of MLN.

ADC can also be determined by using more than two b-values, as we have investigated in this study. Although this approach can improve the robustness and reliability of ADC, multiple b-values lead to longer acquisition times and increased vulnerability to patient motion, both of which can be problematic clinically. Our results indicate that an optimal selection of two b-values can provide similar performance to the approach with multiple b-values, facilitating a time-efficient DWI acquisition in clinical settings.

A limitation of this study is that DWI with b-values larger than 1000 s/mm^2 was not investigated. At a higher b-value, non-Gaussian diffusion phenomena can be observed, leading to a wealth of information on tissue microstructures and heterogeneities [17,23–28].

This represents a direction for future studies. Another limitation is that we did not compare our results with the results from the IVIM model [5]. Such a comparison may provide new insights into the optimal use of information from DWI acquisitions. In addition, PET-CT is another widely used noninvasive diagnostic tool for evaluating mediastinal lymph node. The present study did not compare DWI with PET-CT. Lastly, the sample size of this study was small and lacked an external validation.

In conclusion, we have observed that ADC obtained from b-value pairs of (0, 800), (0, 1000), and (50, 800) s/mm^2 showed superior diagnostic performance compared to the other b-value combinations investigated in this study. Among the three combinations, b-value pair of (50, 800) s/mm^2 appears to be optimal because of its reduced sensitivity to perfusion perturbations as well as advantage in SNR. These results are expected to provide a useful guidance to conduct DWI with two b-values for differential diagnosis of MLN in clinical settings.

Author contribution statement

Li-Ping Qi: Conceived and designed the experiments; Performed the experiments; Analyzed and interpreted the data; Contributed reagents, materials, analysis tools or data; Wrote the paper.

Zheng Zhong: Performed the experiments; Wrote the paper.

Ying-Shi Sun: Analyzed and interpreted the data; Wrote the paper.

Xiao-Ting Li: Performed the experiments; Analyzed and interpreted the data; Contributed reagents, materials, analysis tools or data; Wrote the paper.

Lei Tang: Analyzed and interpreted the data; Contributed reagents, materials, analysis tools or data; Wrote the paper.

Xiaohong Joe Zhou, PhD: Conceived and designed the experiments; Analyzed and interpreted the data; Wrote the paper.

Data availability statement

Data will be made available on request.

Grant support

This work was supported in part by Key Laboratory of Carcinogenesis and Translational Research, Ministry of Education, Peking University Cancer Hospital and Institute, China (Program No: 1122-01-1431). XJZ was not supported by or associated with this grant.

Institutions where work originated

(a) Departments of Radiology, Key Laboratory of Carcinogenesis and Translational Research, Ministry of Education, Peking University Cancer Hospital and Institute;
(b) Center for Magnetic Resonance Research, University of Illinois at Chicago.

The institutional review board of (a) approved this study.

Declaration of competing interest

The authors declare that they have no known competing financial interests or personal relationships that could have appeared to influence the work reported in this paper.

References

[1] A.A. Malayeri, R.H. El Khouli, A. Zaheer, et al., Principles and applications of diffusion-weighted imaging in cancer detection, staging, and treatment follow-up, Radiographics 31 (6) (2011) 1773–1791, https://doi.org/10.1148/rg.316115515. PMID: 21997994; PMCID: PMC8996338.
[2] P. Koşucu, C. Tekinbaş, M. Erol, et al., Mediastinal lymph nodes: assessment with diffusion-weighted MR imaging, J. Magn. Reson. Imag. 30 (2) (2009) 292–297, https://doi.org/10.1002/jmri.21850. PMID: 19629990.
[3] J. Peerlings, E.G. Troost, P.J. Nelemans, et al., The diagnostic value of MR imaging in determining the lymph node status of patients with non-small cell lung cancer: a meta-analysis, Radiology 281 (1) (2016) 86–98, https://doi.org/10.1148/radiol.2016151631. PMID:27110732.
[4] G. Shen, Y. Lan, K. Zhang, et al., Comparison of 18F-FDG PET/CT and DWI for detection of mediastinal nodal metastasis in non-small cell lung cancer: a meta-analysis, PLoS One 12 (3) (2017), e0173104, https://doi.org/10.1371/journal.pone.0173104. PMID: 28253364; PMCID: PMC5333854.
[5] L.P. Qi, W.P. Yan, K.N. Chen, et al., Discrimination of malignant versus benign mediastinal lymph nodes using diffusion MRI with an IVIM model, Eur. Radiol. 28 (3) (2018) 1301–1309, https://doi.org/10.1007/s00330-017-5049-8.
[6] L. Xu, J. Tian, Y. Liu, et al., Accuracy of diffusion-weighted (DW) MRI with background signal suppression (MR-DWIBS) in diagnosis of mediastinal lymph node metastasis of nonsmall-cell lung cancer (NSCLC), J. Magn. Reson. Imag. 40 (1) (2014) 200–205, https://doi.org/10.1002/jmri.24343. PMID: 24923480.
[7] A.R. Padhani, G. Liu, D.M. Koh, et al., Diffusion-weighted magnetic resonance imaging as a cancer biomarker: consensus and recommendations, Neoplasia 11 (2) (2009) 102–125, https://doi.org/10.1593/neo.81328. PMID: 19186405; PMCID: PMC2631136.
[8] I. Joo, J.M. Lee, J.K. Han, et al., Intravoxel incoherent motion diffusion-weighted MR imaging for monitoring the therapeutic efficacy of the vascular disrupting agent CKD-516 in rabbit VX2 liver tumors, Radiology 272 (2) (2014) 417–426, https://doi.org/10.1148/radiol.14131165. PMID:24697148.
[9] C. Schmid-Tannwald, A. Oto, M.F. Reiser, et al., Diffusion-weighted MRI of the abdomen: current value in clinical routine, J. Magn. Reson. Imag. 37 (1) (2013) 35–47, https://doi.org/10.1002/jmri.23643. PMID: 23255414.
[10] D.M. Koh, T. Takahara, Y. Imai, et al., Practical aspects of assessing tumors using clinical diffusion-weighted imaging in the body, Magn. Reson. Med. Sci. 6 (4) (2007) 211–224, https://doi.org/10.2463/mrms.6.211. PMID: 18239358.

[11] W. Chen, W. Jian, H.T. Li, et al., Whole-body diffusion-weighted imaging vs. FDG-PET for the detection of non-small-cell lung cancer. How do they measure up? Magn. Reson. Imaging 28 (5) (2010) 613–620, https://doi.org/10.1016/j.mri.2010.02.009. PMID: 20418042.
[12] J. Nakayama, K. Miyasaka, T. Omatsu, et al., Metastases in mediastinal and hilar lymph nodes in patients with non-small cell lung cancer: quantitative assessment with diffusion-weighted magnetic resonance imaging and apparent diffusion coefficient, J. Comput. Assist. Tomogr. 34 (1) (2010) 1–8, https://doi.org/10.1097/RCT.0b013e3181a9cc07. PMID: 20118713.
[13] Y. Fukukura, T. Shindo, H. Hakamada, et al., Diffusion-weighted MR imaging of the pancreas: optimizing b-value for visualization of pancreatic adenocarcinoma, Eur. Radiol. 26 (10) (2016) 3419–3427, https://doi.org/10.1007/s00330-015-4174-5. Epub 2016 Jan 6. PMID:26738506.
[14] Z. Koc, G. Erbay, Optimal b value in diffusion-weighted imaging for differentiation of abdominal lesions, J. Magn. Reson. Imag. 40 (3) (2014) 559–566, https://doi.org/10.1002/jmri.24403. PMID: 24115207.
[15] Q. Min, K. Shao, L. Zhai, et al., Differential diagnosis of benign and malignant breast masses using diffusion-weighted magnetic resonance imaging, World J. Surg. Oncol. 13 (2015) 32, https://doi.org/10.1186/s12957-014-0431-3. PMID: 25889380; PMCID: PMC4328303.
[16] R. Woodhams, Y. Inoue, S. Ramadan, et al., Diffusion-weighted imaging of the breast: comparison of b-values 1000 s/mm^2 and 1500 s/mm^2, Magn. Reson. Med. Sci. 12 (3) (2013) 229–234, https://doi.org/10.2463/mrms.2012-0028. PMID:23857152.
[17] Y. Sui, H. Wang, G. Liu, et al., Differentiation of low- and high-grade pediatric brain tumors with high b-value diffusion-weighted MR imaging and a fractional order calculus model, Radiology 277 (2) (2015) 489–496, https://doi.org/10.1148/radiol.2015142156. PMID:26035586; PMCID: PMC4627432.
[18] K. Usuda, S. Maeda, N. Motono, et al., Diagnostic performance of diffusion weighted imaging for multiple hilar and mediastinal lymph nodes with FDG accumulation, Asian Pac. J. Cancer Prev. APJCP 16 (15) (2015) 6401–6406, https://doi.org/10.7314/apjcp.2015.16.15.6401. PMID: 26434850.
[19] A.A. Abdel Razek, S. Elkammary, A.S. Elmorsy, et al., Characterization of mediastinal lymphadenopathy with diffusion-weighted imaging, Magn. Reson. Imaging 29 (2) (2011 Feb) 167–172, https://doi.org/10.1016/j.mri.2010.08.002. PMID: 20951522.
[20] W. Junping, S. Tongguo, Z. Yunting, et al., Discrimination of axillary metastatic from nonmetastatic lymph nodes with PROPELLER diffusion-weighted MR imaging in a metastatic breast cancer model and its correlation with cellularity, J. Magn. Reson. Imag. 36 (3) (2012) 624–631, https://doi.org/10.1002/jmri.23695. PMID: 22570219.
[21] M. Iima, D. Le Bihan, Clinical intravoxel incoherent motion and diffusion MR imaging: past, present, and future, Radiology 278 (1) (2016) 13–32, https://doi.org/10.1148/radiol.2015150244. PMID: 26690990.
[22] K. Karki, G.D. Hugo, J.C. Ford, et al., Estimation of optimal b-value sets for obtaining apparent diffusion coefficient free from perfusion in non-small cell lung cancer, Phys. Med. Biol. 60 (20) (2015) 7877–7891, https://doi.org/10.1088/0031-9155/60/20/7877. PMID:26406921; PMCID: PMC4610399.
[23] Y. Sui, Y. Xiong, J. Jiang, et al., Differentiation of low- and high-grade gliomas using high b-value diffusion imaging with a non-Gaussian diffusion model, AJNR Am J Neuroradiol 37 (9) (2016) 1643–1649, https://doi.org/10.3174/ajnr.A4836. PMID: 27256851; PMCID: PMC5018419.
[24] M.M. Karaman, Y. Sui, H. Wang, et al., Differentiating low- and high-grade pediatric brain tumors using a continuous-time random-walk diffusion model at high b-values, Magn. Reson. Med. 76 (4) (2016) 1149–1157, https://doi.org/10.1002/mrm.26012. PMID: 26519663; PMCID: PMC4852163.
[25] L. Tang, Y. Sui, Z. Zhong, et al., Non-Gaussian diffusion imaging with a fractional order calculus model to predict response of gastrointestinal stromal tumor to second-line sunitinib therapy, Magn. Reson. Med. 79 (3) (2018) 1399–1406, https://doi.org/10.1002/mrm.26798. PMID:28643387; PMCID: PMC5741547.
[26] C. Tamura, H. Shinmoto, S. Soga, et al., Diffusion kurtosis imaging study of prostate cancer: preliminary findings, J. Magn. Reson. Imag. 40 (3) (2014) 723–729, https://doi.org/10.1002/jmri.24379. PMID: 24924835.
[27] S. De Santis, A. Gabrielli, M. Palombo, et al., Non-Gaussian diffusion imaging: a brief practical review, Magn. Reson. Imaging 29 (10) (2011) 1410–1416, https://doi.org/10.1016/j.mri.2011.04.006. PMID:21601404.
[28] L. Tang, X.J. Zhou, Diffusion MRI of cancer: from low to high b-values, J. Magn. Reson. Imag. 49 (1) (2019) 23–40, https://doi.org/10.1002/jmri.26293. PMID: 30311988; PMCID: PMC6298843.